International Journal of Solids and Structures 85–86 (2016) 125–133

Contents lists available at ScienceDirect

International Journal of Solids and Structures

journal homepage: www.elsevier.com/locate/ijsolstr

Mechanics of polycarbonate in biaxial impact loading

J.P. Torres*, P.M. Frontini

Institute of Materials Science and Technology (INTEMA), Universidad Nacional de Mar del Plata, J. B. Justo 4302, Mar del Plata 7600, Argentina

ARTICLE INFO

Article history:
Received 13 October 2015
Revised 23 December 2015
Available online 15 February 2016

Keywords:
Biaxial impact
Polycarbonate
Constitutive modeling
Finite element analysis
Failure criteria

ABSTRACT

We investigate the deformation and failure behavior of Polycarbonate (PC) under low-velocity biaxial impact loading. For this, we have conducted experiments and numerical simulations of the falling weight impact test (FWT) for different testing configurations. To model PC behavior in dynamic situations, we employed a 3D thermomechanical constitutive model that captures the strain rate, pressure and temperature dependence of deformation response. The finite element model also incorporates adiabatic heating and contact friction effects. Numerical predictions of the FWT force–displacement curves are in good agreement with experimental observations. An assessment of the developed stress–strain fields indicates that the effective plastic stretch λ_p is the invariant that most suitably represents the point of material failure in all different test configurations. We examine the relation of a maximum λ_p fracture criterion with existing criteria for PC on the grounds of the triaxiality conditions specific to the biaxial impact test. Finally, we propose an extension of these criteria to enhance their capability of predicting failure in part geometries that may become subjected to more complex multiaxial loading scenarios.

1. Introduction

Polycarbonate (PC) is an amorphous polymer widely used in impact resistance demanding applications such as electronic components, exterior automotive and aircraft components, safety helmets and vandal-proof windows. This makes the prediction of the impact response of a PC component in low-velocity impact situations (such as accidental dropping or crashing) a relevant topic from a technological perspective. The instrumented falling weight impact test (FWT) is frequently used to determine the performance of polymers under impact conditions and gain some information of material properties such as strength, ductility, toughness and energy absorption. This test is of technological interest since it develops a stress state in the specimen which closely represents the conditions that arise when loading shell-like components. However, the data obtained in this test are limited since it does not quantify exclusively the material intrinsic behavior but rather the combination of part geometry, loading conditions and material response. To this day, there are no direct procedures to use FWT results for quantitative structural design and prediction. As a consequence, the FWT is mostly used as a pass/fail test or to perform qualitative comparisons of material impact resistance. A more detailed understanding of polymer mechanical response in the FWT can be achieved by carrying out full 3D finite element simulations and relating the resulting stress–strain fields with loading conditions. In order to carry out quantitative predictions of the impact performance of plastics, the material intrinsic deformation behavior, i.e., the stress response measured under homogeneous deformation, must be first evaluated and described by proper constitutive relations (Meijer and Govaert, 2005). Currently, a considerable amount of experimental data for PC mechanical behavior at a wide range of temperatures and strain rates is available (Bauwens-Crowet et al., 1972; Hasan and Boyce, 1995; Mulliken and Boyce, 2006; Rietsch and Bouette, 1990). Physically-based 3D constitutive models for PC have been developed by several research groups and they have been refined to capture several features of polymer deformation response including strain rate, temperature and pressure dependence, post-yield softening and large strain entropic hardening (Anand and Gurtin, 2003; Arruda et al., 1995; Bergström and Bischoff, 2010; Boyce et al., 1988; Mulliken and Boyce, 2006; Wu and der Giessen, 1993). Specific to the case of PC under dynamic loading is the model of Mulliken and Boyce (2006). This model accounts for the α–β transition of yield behavior occurring at low temperatures and/or high strain rates (Bauwens-Crowet et al., 1972) and accurately predicted the deformation response of PC from low ($10^{-4}s^{-1}$) to high ($10^{4}s^{-1}$) strain rates in uniaxial compression loading.

* Corresponding author. Tel.: +542234816600.
E-mail address: jptorres@fi.mdp.edu.ar, juantorresmdp@gmail.com (J.P. Torres).

http://dx.doi.org/10.1016/j.ijsolstr.2016.02.010
0020-7683/

1.1. Failure modeling of PC

A number of investigations have dealt with the phenomenological aspects of PC fracture behavior (Ishikawa et al., 1977; Narisawa and Yee, 1993; Nimmer and Woods, 1992). It was found that, depending on the test geometry, PC can exhibit two different fracture mechanisms: (i) ductile fracture, observed in smooth-bar tension or compression experiments, preceded by shear yielding-induced large plastic stretches; and (ii) brittle fracture, present in plain strain notch conditions where a high triaxiality state is developed, favoring crazing over shear-yielding. This difference in response has been found to be related to the hydrostatic stress magnitude resulting from stress concentration ahead of the notch (Gearing, 2002). The majority of studies on PC failure prediction have been undertaken within the framework of fracture mechanics (Estevez et al., 2000; Fraser and Ward, 1977; Newmann and Williams, 1980). An alternative approach using the combination of physically-based constitutive models and failure criteria formulated at the continuum level has been recently proposed (Gearing and Anand, 2004a; 2004b; Kattekola et al., 2013). This means that the fine microstructural features of the fracture process are omitted and are only accounted in an averaged sense, over a microstructural representative volume element. These fracture models are defined as a function of a stress or strain invariant that reaches a critical value and initiates failure. After failure has initiated, either damage evolution laws or direct element removal can be applied. This technique has the potential to be used as a quantitative engineering tool to predict deformation and failure in structures and geometries different to those found in typical standardized tests, where the location of failure initiation is not known *a priori* (Gearing, 2002). Gearing and Anand (2004a); 2004b) used this approach to model fracture in notched four-point bending specimens. They defined a brittle failure criterion based on a critical mean normal stress value σ_m^c,[1] and a ductile failure criterion based on a critical plastic chain stretch value λ_p^c. Then, they incorporated these failure criteria into the model of Anand and Gurtin (2003) and showed that their enhanced constitutive model was able to quantitatively predict both the ductile failure of blunt-notched beams, and competition between ductile and brittle failure in sharply-notched beams in four point bending. These investigations concluded with the recommendation that further research should be carried out to verify the predictive capabilities of this failure modeling approach under different strain-rate, temperature, specimen geometries and loading conditions. Since then, other investigations on PC fracture modeling include the work of Kattekola et al. (2013) on fracture behavior of SEN samples in quasi-static loading, and Faye et al. (2015) on dynamic fracture experiments and simulations of SEN specimens at high velocities. However, the modeling of PC fracture on biaxial impact loading has not been addressed so far.

As a consequence, the objective of this investigation is to provide further empirical support for the validation of the invariant-based failure criteria as a practical engineering tool for modeling PC in low-velocity impact situations. For this, we have conducted biaxial impact falling weight tests and the results were compared with finite element predictions. To model PC behavior in dynamic situations, we employed a physically-based constitutive model that captures the strain rate, pressure and temperature dependence of deformation response. The finite element model also incorporates adiabatic heating and contact friction effects. We assessed material failure modeling using the invariant-based failure criteria of Gearing et al. and an element removal technique. We discuss PC fracture on the grounds of the specific stress–strain states developed in biaxial loading. Finally, we analyze the feasibility of extending these fracture criteria to predict failure in general multiaxial loading scenarios.

[1] The terms "mean normal stress" and "hydrostatic stress" are used in this work indifferently.

2. Problem formulation

2.1. Constitutive model

The constitutive model is based on the kinematic finite strain framework of previous models proposed by Hasan and Boyce (1995), Bergström and Boyce (1998), Mulliken and Boyce (2006) and Bergström and Bischoff (2010) that capture the pressure, temperature and rate dependent elastoplastic response of polymers. The model consists of an arrangement of three separate elements: a linear elastic spring acts in series with a viscoplastic dashpot (network A), and a non-linear Langevin spring acts in parallel to both (network B). The linear spring and dashpot captures the initial elastic response followed by rate-dependent plastic flow originated by intermolecular resistance to chain-segment rotation (Boyce et al., 1988). The Langevin spring models the strain-hardening response at large deformations caused by entropic resistance to chain alignment (Arruda and Boyce, 1993). This model works as a simplification of the Mulliken–Boyce (MB) model (Mulliken and Boyce, 2006) whereby instead of using two separate spring-dashpot elements to model the α and β mechanisms over a wide range of strain-rates, we concentrate them into a single element that is calibrated to fit PC behavior in the 10^0–$10^3 s^{-1}$ strain-rate range. This narrower range is specific to that found in FWT.

Fig. 1 shows a schematic rheological representation of the constitutive model. Since networks A and B act in parallel, the total stress $\mathbf{T}$ and deformation gradient $\mathbf{F} \equiv \partial \mathbf{x}/\partial \mathbf{X}$, are given by:

$$\mathbf{T} = \mathbf{T}_A + \mathbf{T}_B \tag{1}$$

and

$$\mathbf{F} = \mathbf{F}_A = \mathbf{F}_B \tag{2}$$

In addition, the deformation gradient in network A may be multiplicatively decomposed into elastic and plastic components (Lee, 1969)

$$\mathbf{F}_A = \mathbf{F}_A^e \mathbf{F}_A^p \tag{3}$$

The rate of change of the plastic deformation gradient, $\dot{\mathbf{F}}_A^p$, is related to the rate of shape change tensor $\mathbf{D}_A^p$ through

$$\dot{\mathbf{F}}_A^p = \mathbf{D}_A^p \mathbf{F}_A^p \tag{4}$$

Where $\mathbf{D}_A^p = \left(\mathbf{L}_A + \mathbf{L}_A^T\right)/2$, and $\mathbf{L}$ is the velocity gradient $\partial \mathbf{v}/\partial \mathbf{x}$, which is assumed to be irrotational. The direction of $\mathbf{D}_A^p$ is assumed to be coaxial with the deviatoric stress acting on network A:

$$\mathbf{D}_A^p = \dot{\gamma}^p \frac{\mathbf{T}_A'}{\tau} \tag{5}$$

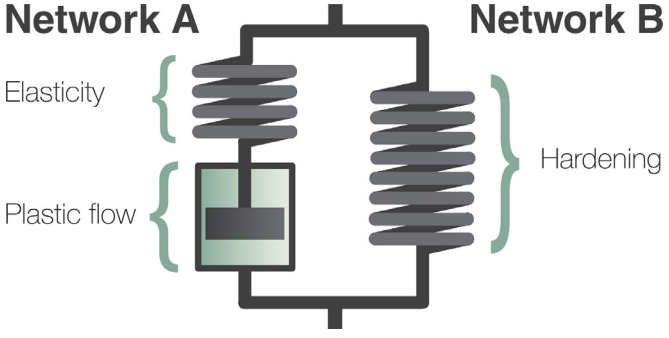

Fig. 1. 1-D rheological representation of the constitutive model.

Where $\mathbf{T}_A^{'} = \text{dev}[\mathbf{T}_A]$ and $\tau = \sqrt{\text{tr}[\mathbf{T}_A^{'}\mathbf{T}_A^{'}]/2}$ is the equivalent applied shear stress. The magnitude of $\mathbf{D}_A^p$ is then defined by the plastic strain rate $\dot{\gamma}^p$.

Equations (1) –(5) define the general kinematics. The material-specific behavior is defined next by providing constitutive laws that relate the acting stresses, $\mathbf{T}_A$ and $\mathbf{T}_B$, with the deformation response, $\mathbf{F}_A$ and $\mathbf{F}_B$.

The stress acting on network A is given by the linear elastic constitutive law:

$$\mathbf{T}_A = \frac{f_\theta^e}{J^e}\left(2\mu^e \mathbf{E}_A^e + \lambda^e \ \text{tr}[\mathbf{E}_A^e]\mathbf{I}\right) \tag{6}$$

Where $J^e = \det[\mathbf{F}_A^e]$, $\mathbf{E}_A^e = \ln[\mathbf{V}_A^e]$ is the logarithmic true strain or Hencky strain (derived from the left stretch tensor of $\mathbf{F}_A^e$: $\mathbf{V}_A^e = \sqrt{\mathbf{F}_A^e(\mathbf{F}_A^e)^T}$), $\mathbf{I}$ is the second-order identity tensor, μ^e and λ^e are Lamé constants, the function f_θ^e models linear temperature dependence and is given by:

$$f_\theta^e(\theta) = \left[1 + q_\theta^e\left(\frac{\theta - \theta_0}{\theta_0}\right)\right] \tag{7}$$

Where θ is the current temperature, θ_0 is the reference temperature and q_θ^e is the temperature scaling factor. The stress acting on the non linear strain-hardening spring on network B is given by the Arruda–Boyce eight-chain model (Arruda and Boyce, 1993; Bergström and Boyce, 1998):

$$\mathbf{T}_B = \frac{\mu_\text{h}}{J\overline{\lambda^*}}\frac{\mathcal{L}^{-1}(\overline{\lambda^*}/\lambda_L)}{\mathcal{L}^{-1}(1/\lambda_L)}\text{dev}[\mathbf{B}^*] + \kappa(J-1)\mathbf{I} \tag{8}$$

μ is the shear modulus, λ_L is the locking stretch, $\mathbf{B}^* = J^{-2/3}\mathbf{F}\mathbf{F}^T$ is the distortional part of the left Cauchy–Green tensor, $\overline{\lambda^*} = \sqrt{\text{tr}[\mathbf{B}^*]/3}$, $\mathcal{L}^{-1}(x)$ is the inverse Langevin function and κ is the bulk modulus. The eight-chain model was originally derived to model the hyperelastic behavior of rubbers above their glass transition, which is controlled by the stretch-induced reduction of configurational entropy. Notably, this entropic phenomenon also takes place in glassy polymers at large plastic strains, due to the incremental alignment of molecular segments in the course of continued shear transformations (Argon, 2013). Therefore, it is often convenient to model the large strain hardening of glassy polymers using a straightforward hyperelastic model for rubbers. This approach has been proposed in the ground-breaking works of Haward and Thackray (1968), Argon (1973) and Boyce et al. (1988) and has been successfully applied in numerous models for glassy polymers that followed.

The plastic strain rate $\dot{\gamma}^p$ is related to the stress acting in the viscoplastic element through a power-law relationship:

$$\dot{\gamma}^p = \left(\frac{\tau}{f_{\epsilon^p} f_\theta^p f_p \hat{\tau}}\right)^m \tag{9}$$

Where $\hat{\tau}$ is the shear flow resistance, m is the shear flow exponent. f_{ϵ^p} is a function that captures strain softening after yield according to:

$$f_{\epsilon^p} = f_f + (1 - f_f)\exp\left[\frac{-\epsilon_p}{\hat{\epsilon}}\right] \tag{10}$$

Where $\epsilon_\text{vm}^p = \sqrt{2/9\left[(\epsilon_1^p - \epsilon_2^p)^2 + (\epsilon_2^p - \epsilon_3^p)^2 + (\epsilon_3^p - \epsilon_1^p)^2\right]}$ is the applied effective Mises plastic strain, ϵ_i^p are the principal values of $\ln[\mathbf{B}^p]$, f_f is the final value of $\hat{\tau}$ after softening and $\hat{\epsilon}$ is the characteristic transition strain. f_θ^p is a function that models the linear temperature dependence of the viscoplastic element according to:

$$f_\theta^p(\theta) = \left[1 + q_\theta^p\left(\frac{\theta - \theta_0}{\theta_0}\right)\right] \tag{11}$$

Table 1
Constitutive parameters for the proposed model.

Property	Parameters	Constants
Elastic	μ^e (MPa)	750
	λ^e (MPa)	2375
Viscoplastic	$\hat{\tau}$ (MPa)	48.6
	m	11.3
Softening	f_f	0.38
	$\hat{\epsilon}$	0.16
Hardening	μ (MPa)	39.2
	λ_L	2.3
Pressure dependence	$\tau_{t/c}$	2.18
Temperature dependence	q_θ^e	-0.9
	q_θ^p	-2.0
Thermal	ω	0.6
	k (W/m · K)	0.2
	C_p (kJ/kg · K)	1.25
Friction	μ_k	0.4

Where θ, θ_0 and q_θ^p are defined in a similar fashion to Equation (7). Finally, pressure dependence of the flow element is given by the function f_p:

$$f_p = r\tau_{t/c} + (1 - r) \tag{12}$$

where the parameter r is given by: $r = 0$, if $(\text{tr}[\mathbf{T}]/\sigma_\text{vm} \leq -1)$; $r = 1$, if $(\text{tr}[\mathbf{T}]/\sigma_\text{vm} \geq 1)$; or $r = \text{tr}[\mathbf{T}]/2\sigma_\text{vm} + 1/2$ otherwise.

2.2. Finite element model

Simulations of the falling weight impact test were carried out in ABAQUS/Explicit 6.12 using a fully coupled thermal-stress dynamic analysis step which accounts for inertia effects, transient thermal response and temperature-dependent material response. This analysis involves the simultaneous integration of the momentum equation and the heat flow equation that couples the energy dissipation during plastic flow to the local temperature rise (Hibbit et al., 2012). The thermo-mechanical parameters for the proposed constitutive model are presented in Table 1 and the parameter calibration procedure is described in Appendix. The constitutive model is incorporated in ABAQUS as user material subroutine VUMAT using the commercial PolyUMod® library (Bergström, 2012). The PC plate was modeled using (C3D8RT) eight-node thermally coupled brick reduced integration elements. Element size at the disc central region is 0.2 mm and it is coarsened to 2 mm towards the edges (see Fig. 2). The striker was modeled as an analytical rigid surface. Clamping of the specimen was modeled enforcing zero-displacement of the nodes located along the specimen outer-edge. Surface-to-surface contact interaction between the striker and disc

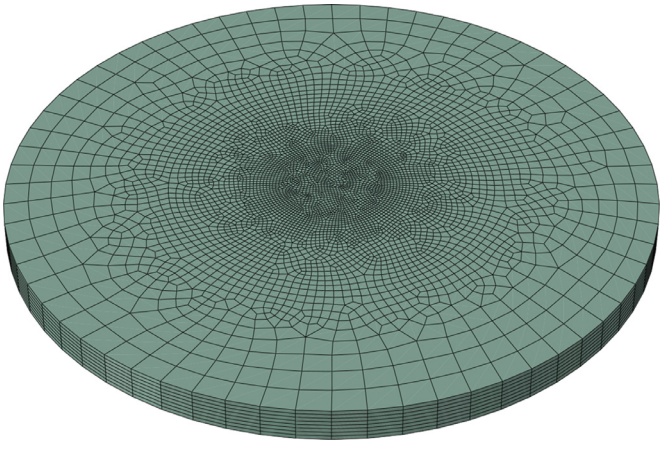

Fig. 2. Element mesh used for the simulations.

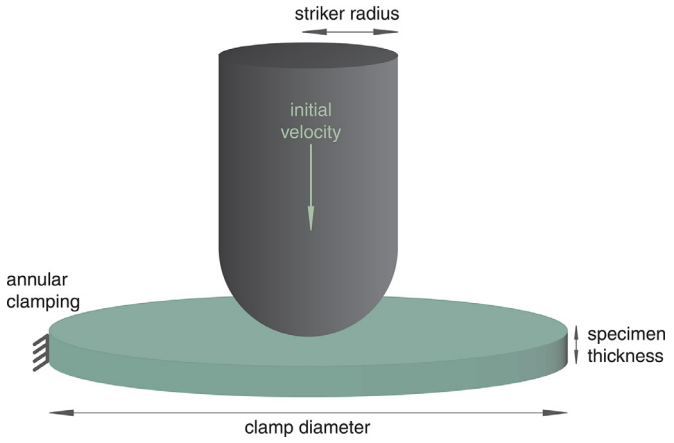

Fig. 3. Falling weight impact test geometry.

was defined using Penalty tangential behavior and hard contact normal behavior. Initial striker velocity and disc temperature were defined using the Predefined Field option. Heat transfer between the specimen and the surrounding media (including the striker) was neglected. Enhanced hourglass control and element distortion control using a 0.01 length ratio were included in order to prevent simulation premature termination due to excessive element distortion. Material failure is modeled using the element deletion technique available in ABAQUS/Explicit. This technique requires the use of an appropriately dense 3D mesh for predictions to be reasonably accurate (Gearing, 2002). Each simulation took approximately 18 h to complete running on an i7 Intel 2.8 GHz processor.

3. Experimental procedure

3.1. Sample preparation

Rectangular specimens were cut from commercial Polycarbonate (Makrolon® GP grade) extruded sheets manufactured by Bayer Material Science LLC. To erase material thermomechanical prehistory, specimens where heated to 15 °C–20 °C above the glass transition temperature and maintained at that temperature for 3 h. Following, the polymer was 'annealed' by cooling slowly to room temperature from 165 °C for about 8 h. This heat treatment was performed under vacuum conditions to eliminate oxidation. Prior to testing, the samples were stored in a desiccator cabinet for three days to remove moisture. The treatment aims to imitate the initial material state used in the works of Bauwens-Crowet et al. (1972), Mulliken (2004), and Mulliken and Boyce (2006) from which the constitutive material parameters where determined.

3.2. Impact testing

Low-velocity FWT impact testing was carried out in an instrumented falling weight testing machine (Fractovis Ceast 6789) using a 23.7 kg striker mass and at 4.3 m/s impact velocity. In this test, a circular plate specimen is placed horizontally and clamped on its outer edges by an annular support. Then, a vertically free-falling spherical striker hits the specimen on its center (see Fig. 3). The striker is equipped with Wheatstone bridge based strain gage force sensor that is connected to a Ceast DAS 4000 data acquisition system. The sensor measures the load on the striker and records it as a function of time. Data acquisition rate is of 1 μs with 300 kHz band-pass. Sensor sensitivity and natural frequency are 10 N and 8 kHz respectively.

Different testing configurations were used to impose non-identical stress-strain field distributions (see Table 2). Molikote lubricant was used for tests using lubricated surfaces. All tests were conducted at ambient temperature. To verify the repeatability of the load-time curve and failure response, tests for each configuration were replicated five times. After failure, scanning electron microscopy (SEM) was carried out in the specimen fractured surfaces using a Jeol JSM-6460LV microscope.

Table 2
Impact testing configurations.

Thickness (mm)	Surface condition	Striker radius (mm)	Clamp diameter (mm)	Case name
2.1	Lubricated	40	10	2-40-lub
		76	6.35	2-76-lub
	Non-lubricated	40	10	2-40-fric
		76	6.35	2-76-fric
5.0	Lubricated	40	10	5-40-lub
		76	6.35	5-76-lub

4. Results and discussion

4.1. Pre-failure analysis

The prediction capability of the constitutive model is first assessed by comparing experimental and simulated force–time curves. For all testing configurations, good agreement between experiments and simulations is observed. Results are shown in Fig. 4 for tests 2-40-lub and 2-40-fric (tests with and without surface lubrication) and Fig. 5 for tests 2-40-fric and 2-76-fric (tests varying clamp and striker geometry). In every case, experimental curves

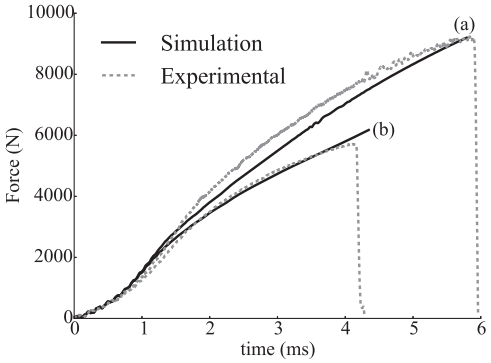

Fig. 4. FWT force–time experimental and FEM prediction curves for 2.1 mm plates. (a) Tested with no lubricant, modeled using $\mu_k = 0.4$; (b) tested with lubricant, modeled using frictionless contact.

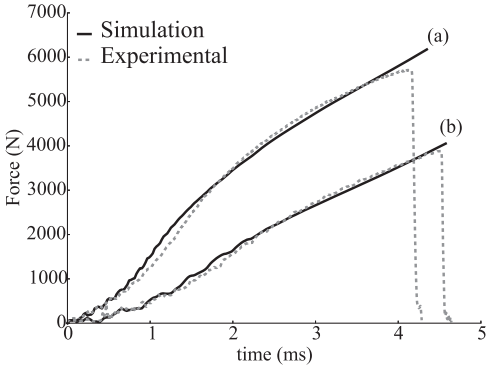

Fig. 5. FWT force–time experimental and FEM prediction curves for 2.1 mm plates (without lubrication). (a) Clamp diameter = 40 mm, striker radius = 10 mm; (b) clamp diameter = 76 mm, striker radius = 6.35 mm.

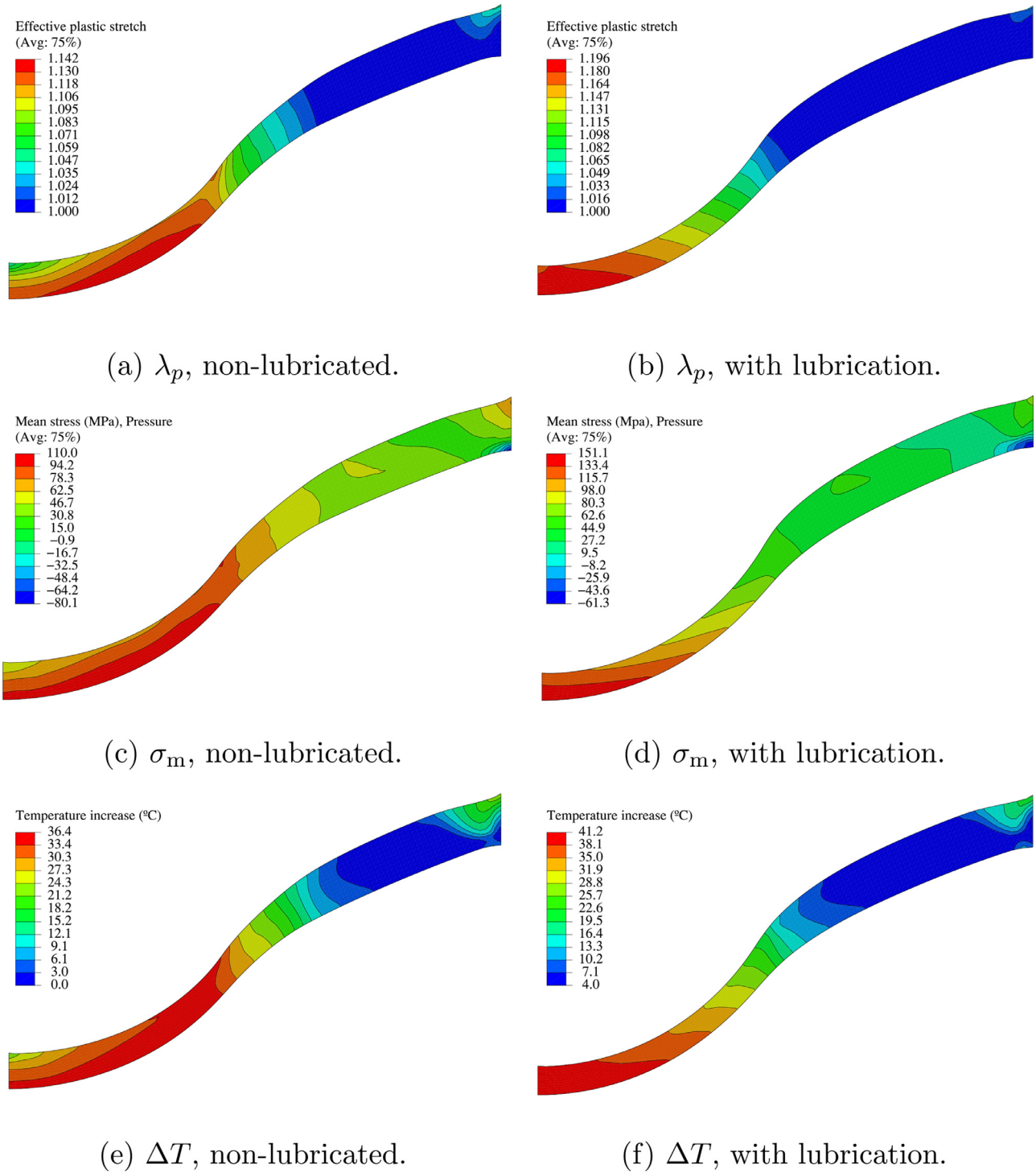

Fig. 6. Effective plastic stretch λ_p, mean stress σ_m and temperature increase ΔT distributions for 2.1 mm specimens (striker diameter = 20 mm; clamp diameter = 40 mm; impact velocity = 4.3 m/s.).

show monotonically increasing force values followed by a sharp drop caused by catastrophic failure in the specimen. The effect of lubricant is depicted in Fig. 4, where it can be observed that friction between specimen and striker produces an increase both in impact load and fail time. Fig. 5 shows the effect of clamp diameter and striker size. A larger clamp diameter produces a structure that is more bending compliant which results in a smaller impact force at failure.

FEM simulations also allow to study the full 3D stress, strain, strain-rate and temperature fields developed in the specimen. Fig. 6 shows the effective plastic stretch λ_p, mean stress σ_m and temperature increase ΔT fields at the moment of failure. In frictionless impact, the maximum principal stress and strain values are located on the face opposite to the striker contact surface and in the center of the specimen. On the other hand, friction between the specimen and the striker causes localization of both stress and

Table 3
Field values at failure.

Case	λ_p	ϵ_I	ϵ_{vm}	σ_m (MPa)	σ_I (MPa)	σ_{vm} (MPa)	σ_m/σ_{vm}	ΔT_{max} (°C)	$\langle\dot{\epsilon}\rangle$ (s^{-1})	t_{fail}(ms)
2-40-lub	1.198	0.767	1.419	151	228	230	0.66	41	238	4.39
2-40-fric	1.146	0.778	1.189	110	205	191	0.63	35	183	5.55
2-76-lub	1.235	0.853	1.563	190	288	292	0.65	45	186	4.62
2-76-fric	1.154	0.789	1.230	116	204	196	0.65	37	260	5.32
5-40-lub	1.252	0.889	1.624	211	320	327	0.65	44	189	5.41
5-76-lub	1.254	0.894	1.632	217	329	335	0.65	47	267	6.82
Mean	1.206	0.828	1.443	166	262	262	-	41.5	220	-
σ_{sd}	0.048	0.057	0.197	46.8	57.1	64.6	-	4.7	39	-

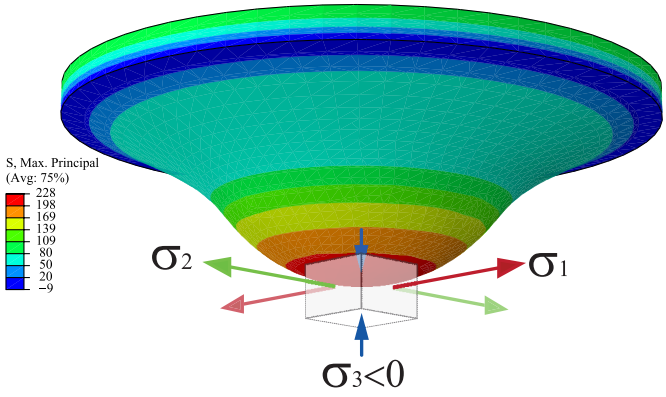

Fig. 7. Principal stresses directions in a volume element located at the disc center. σ_1 and σ_2 are positive radial while σ_3 is negative compressive in the loading direction.

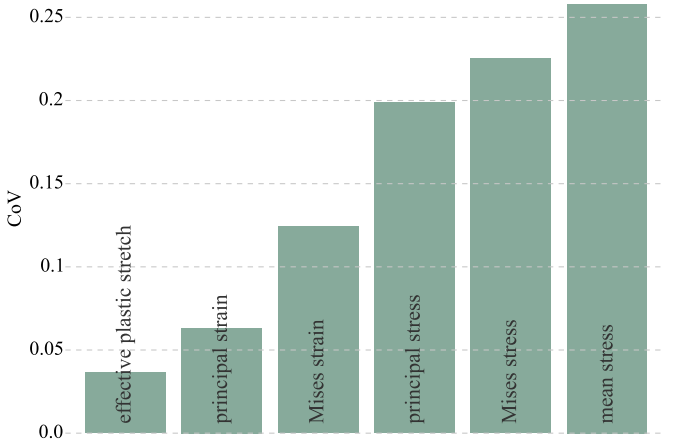

Fig. 8. CoV of maximum values of stress–strain based invariants at failure time. the effective plastic stretch λ_p shows the lowest variability among the different test configurations.

strain in an annular region shifted from the disc center. It is clear that this shift is caused by the shearing frictional force developed on the contact surface. Temperature rise due to adiabatic heating is between 35 °C and 47 °C depending on the test configuration (see Table 3), this has an effect in material response that cannot be neglected. Although we do not show the curves here, we found that not accounting for adiabatic heating produces an overestimation in the force values of approximately 20%. Strain-rate $\dot{\epsilon}$ evolution is dependent of both geometry and contact conditions. Volume-averaged values are in the range of 50–300 s^{-1} (though a local $\dot{\epsilon}$ up to 700 s^{-1} was observed in the elements located at the disc center). These values are within the range that was chosen to calibrate material parameters (see Appendix).

4.2. Material failure analysis

PC samples show catastrophic failure as evidenced by the sharp drop in the force–time curves. The dispersion in the observed time to failure t_f for each testing configuration is approximately 5%. Table 3 shows values, at failure time t_{fail}, of field invariants previously used to define failure criteria in polymers (Bergström et al., 2005; Gearing and Anand, 2004a, 2004b): effective plastic chain stretch, $\lambda_p = \sqrt{\mathrm{tr}[\mathbf{B}^p]/3}$; effective Mises plastic strain ϵ^p_{vm} (defined in Equation (10)) ; principal Logarithmic strain, ϵ_I; mean stress, $\sigma_m = \mathrm{tr}[\mathbf{T}]/3$; principal stress, σ_I and Von Mises stress σ_{vm}. In addition, Table 3 reports stress triaxiality σ_m/σ_{vm} at the maximum σ_m location; maximum temperature increase ΔT_{max} at the maximum λ_p location; and the maximum principal strain rate values $\langle\dot{\epsilon}\rangle$ averaged in a circular region of radius equal to the striker radius. Fig. 8 shows the scatter associated with each invariant, quantified using the coefficient of variation CoV, i.e., the ratio of the standard deviation σ_{sd} to the mean value ratio μ_{mean}. λ_p shows the lowest variability among the different test configurations (below 5%).

A competition between brittle and ductile failure of notched PC specimens has been previously observed in tensile (Gearing and Anand, 2004a; Smit et al., 2000), three-point bending (Ishikawa et al., 1977; Nimmer and Woods, 1992) and four-point bending (Gearing and Anand, 2004a) tests. The high triaxial stress fields ahead of the notch were assumed to play the key role in the nucleation of cracks and a maximum hydrostatic tension was proposed as a failure criterion, i.e. brittle failure will occur when $\sigma_m > \sigma^c_m$, where σ^c_m is the critical mean normal stress. They determined a σ^c_m value in the range 80–100 MPa. For the case of biaxial impact loading, our analysis of the mean normal stress show that the σ^c_m is reached before the point of experimental observed failure (mean σ_m at t_f is 166 MPa and it shows a variability of ≈25% among the different test configurations, see Fig. 8). The reason for this is that, although a high level of hydrostatic tension is developed in biaxial loading, this does not occur due to a high stress triaxiality but because both the maximum principal (radial) and mid-principal (circumferential) stresses are high, while the minimum principal (through-thickness) stress is negative and close to zero (see Fig. 7). It is reasonable to expect then that any cavitation/crack-nucleation phenomena will be inhibited since volumetric expansion requires driving stresses in all three principal directions and not only on a 2D surface. Therefore, it can be suggested that the σ^c_m failure criteria cannot be generalized to geometries where low triaxiality states at high hydrostatic tension levels are developed. In other words, the hydrostatic tension level alone is not always a suitable magnitude to quantify dilational stress triaxiality. This consideration is important for performing FEM predictions of PC failure in more complex structures and loading conditions, where the triaxiality levels are difficult to anticipate. Nevertheless, the σ^c_m criterion could be constrained by adding the condition that the stress triaxiality factor σ_m/σ_{vm} should be higher than a certain threshold

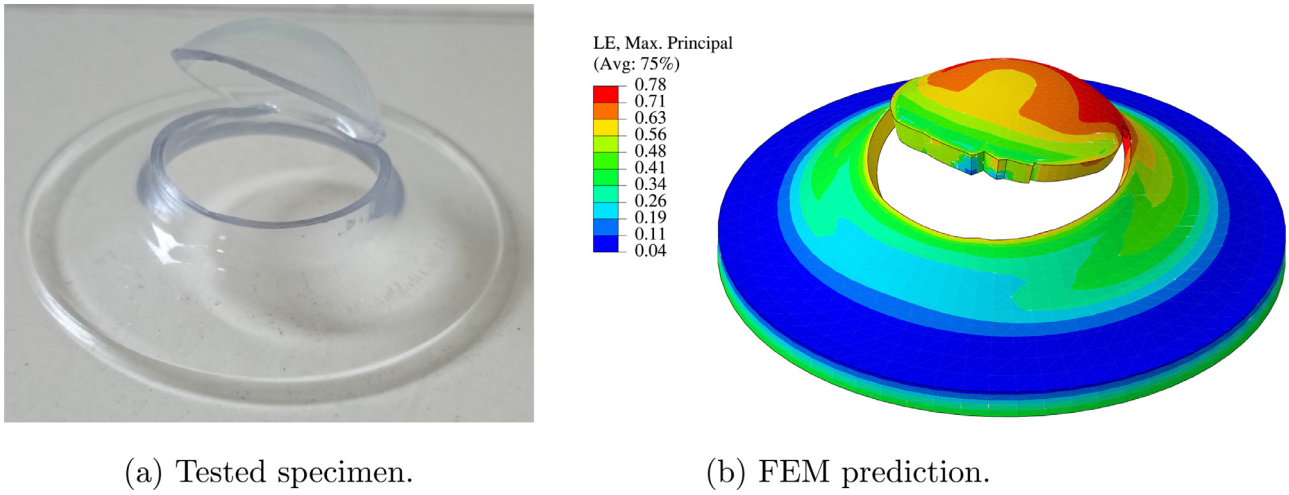

Fig. 9. Fracture aspect of the FWT specimens tested using no lubricant.

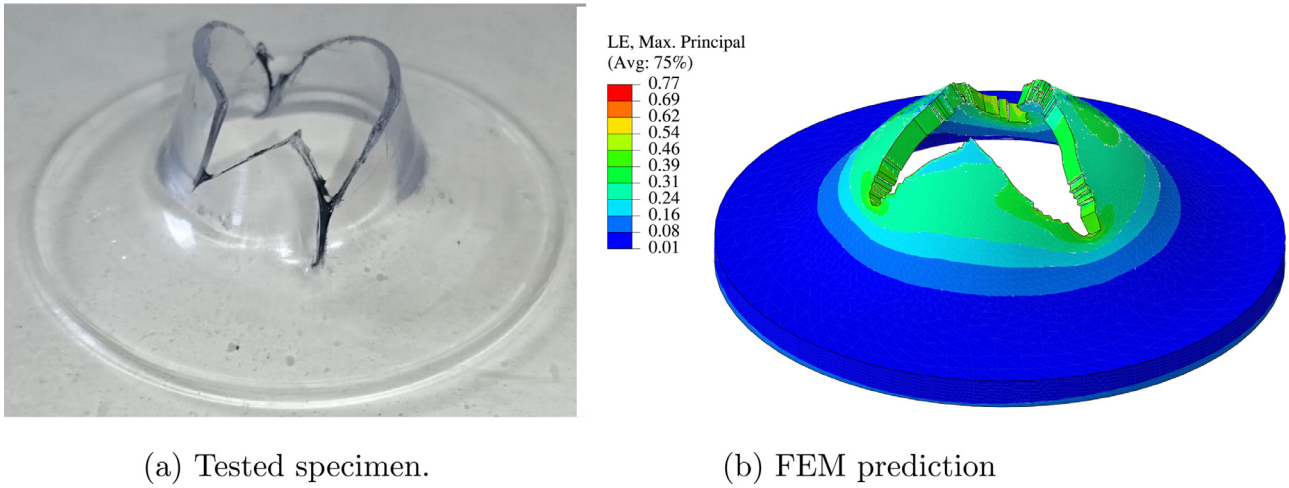

Fig. 10. Fracture aspect of the FWT specimens tested using lubrication.

value. Table 3 shows that σ_m/σ_{vm} values are approximately 0.65. Tiejun et al. (2002) analyzed the fracture behavior of PC tensile notched bars for varying notch radius and observed ductile failure at low and medium triaxiality levels ($\sigma_m/\sigma_{vm} = 0.3$ and 0.82 respectively), whereas brittle failure took place at a high stress triaxiality ($\sigma_m/\sigma_{vm} = 1.27$). Although these values are insufficient to establish an accurate stress triaxiality value, they provide an approximate range where the ductile-to-brittle transition can take place.

Gearing et al. modeled PC ductile failure (Gearing and Anand, 2004a; 2004b) using an effective plastic stretch $\lambda_p = \sqrt{\text{tr}[\mathbf{B}^p]/3}$ failure criterion i.e. failure will occur when $\lambda_p > \lambda_p^c$, where λ_p^c is the critical plastic stretch. They determined a value $\lambda_p^c = 1.192$ from uniaxial tensile tests at 0.0125 mm/s (nominal strain-rate of $10^{-3}s^{-1}$). Table 3 shows the values observed in our FWT simulations for strain-based invariants $\lambda_p, \bar{\lambda}$ and ϵ_I at t_f. The mean λ_p value is 1.206 (showing only a 1.2 % difference with Gearing's value). In addition, we see λ_p shows a lower variability than the other strain measures (see Fig. 8). Table 3 also shows the temperature and strain-rate values in the region where failure is initiated. Here, we see that there is a variation of approximately 5 orders of magnitude in strain-rate and 40 °C in temperature between the tensile tests in Gearing and Anand (2004a) and our impact tests in this study. Keeping in consideration the criterion accuracy both at the strain rates used by Gearing ($\dot{\epsilon} = 10^{-3}s^{-1}$) and the strain rates in this study, it can be suggested that the λ_p^c criterion for ductile failure can be considered strain-rate and temperature independent, at least in a $\dot{\epsilon} = 10^{-4}$–$10^{3}s^{-1}$ and $\Delta T < 50°$ C working range (for initial ambient temperature conditions). Consequently, we performed simulations of PC failure assuming a critical $\lambda_p^c = 1.205$. Figs. 10 and 9 show fracture surface features of tested specimens and FEM predictions. Failure for lubricated specimens initiates at the disc center and propagates radially tearing the material in several ear-shaped flaps. For specimens tested without lubricant, failure initiation at a distance from the disc center results in a circumferential propagating crack that tears the material forming a cap. The main features of specimen failure are predicted by the simulations.[2] The λ_p^c failure criterion is related to a mechanism of ductile tearing preceded by shear-yielding (Gearing and Anand, 2004a). Fig. 11 shows an SEM image of the fracture surface of a failed PC disc corresponding to case 2-40-fric. Surface aspect shows striated lines propagating radially from a fracture initiation point. The presence of well defined striation lines has been related to ductile failure (Chang et al., 1992). *These observations together with our failure simulation results give further support for establish-*

[2] We have checked the sensitivity of the fracture patterns to our mesh size and found that decreasing the element size reproduces the same non-lubricated failure pattern; whereas for frictionless failure, ear-shaped flaps are always reproduced as well, however the paths they take to be formed would differ.

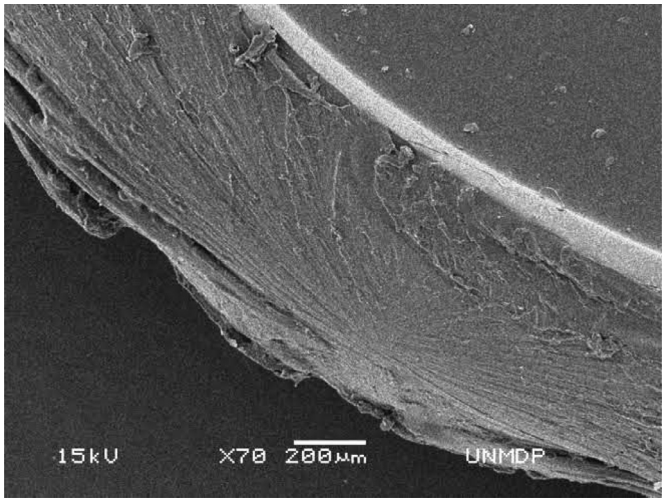

Fig. 11. SEM micrograph of a PC failed disc showing failure by ductile tearing.

ing the effective plastic stretch as a suitable measure for modeling ductile failure of PC in multiaxial impact scenarios.

5. Concluding remarks

We investigated the feasibility of predicting numerically the deformation and failure behavior of Polycarbonate under low-velocity biaxial impact loading. This configuration is technologically relevant since it recreates stress states similar to those developed in shell-like components which undergo accidental drop-falling or crashing. Several testing configurations varying specimen thickness, clamping diameter, striker radius and surface lubrication were used in order to induce different stress–strain states. We carried out finite element simulations incorporating adiabatic heating and friction effects. PC strain-rate, temperature and pressure dependent response is modeled using a proposed 3D thermo-mechanical constitutive model. This model is specifically calibrated to represent the temperature/strain-rate regime developed in FWT using available experimental data in the literature. The model reproduces the overall specimen response before failure as can be seen by contrasting experimental and FEM curves. To model material failure, we assessed the invariant-based fracture criteria of Gearing et al. These criteria capture the competition between brittle (maximum hydrostatic tension σ_{m}^{c}) and ductile (maximum plastic stretch λ_{p}^{c}) failure modes. Key findings of this investigation are:

- An analysis of the hydrostatic stress field in the simulations indicates that the σ_{m}^{c} brittle fracture criterion predicts material failure prematurely. The reason for this is that in biaxial impact, high hydrostatic stresses are developed at low triaxiality levels ($\sigma_{\mathrm{m}}/\sigma_{\mathrm{vm}} \approx 0.65$).
- On the contrary, the λ_{p}^{c} ductile failure criterion using a $\lambda_{p}^{c} \approx 1.205$ value, was found to predict accurately both fail time and macroscopic fracture patterns of experimental samples for all geometrical configurations. This finding provides empirical support to extend the λ_{p}^{c} value to biaxial loading scenarios and to moderately high rate loading (at least to a $\dot{\epsilon} = 10^{-4}$–$10^{3}\mathrm{s}^{-1}$ and $\theta = 20$ °C–65 °C working range).
- If failure modeling of more complex structures and multiaxial loading scenarios is to be performed (where the failure mode cannot be anticipated), the σ_{m}^{c} criterion should be constrained to incorporate a condition in the stress state, e.g.: the σ_{m}^{c} criterion should only be activated if the triaxiality level is above a threshold level. Based on available data, this level should be in the range $0.8 < \sigma_{\mathrm{m}}^{c} < 1.2$. Further research should be carried out to determine a more accurate value.

Appendix. Determination of constitutive parameters

Parameters for the proposed constitutive model were determined from PC experimental and numerical data found in the literature. Fig. A.12 shows a qualitative representation of the data

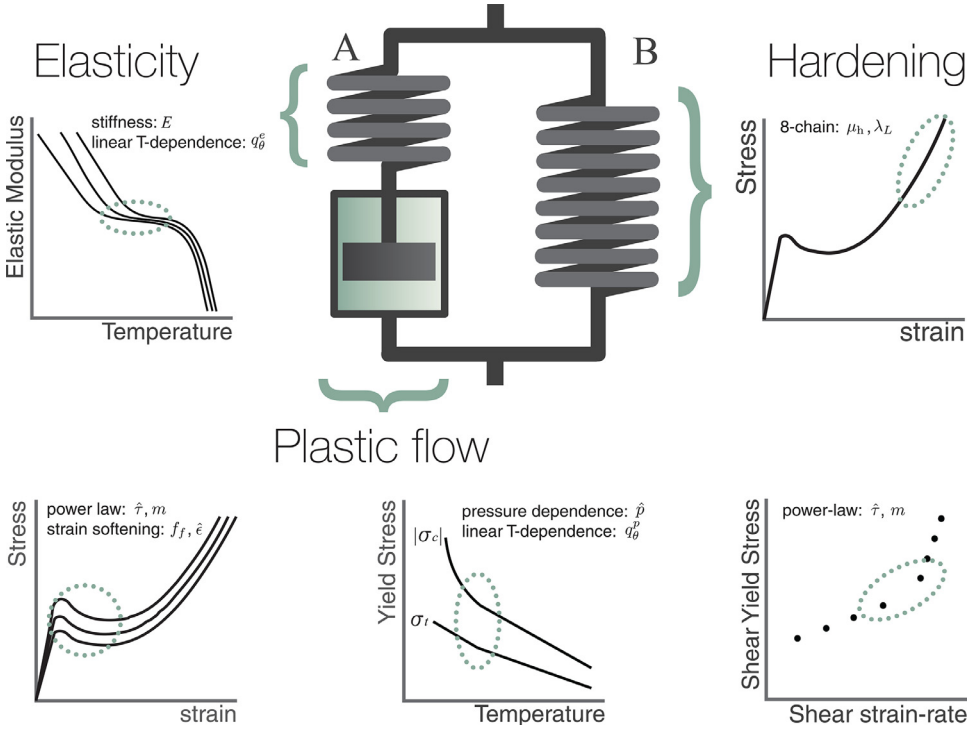

Fig. A12. Schematic representing parameter calibration procedure. The dotted ellipses show the region in which the parameters were calibrated.

used to calibrate the model. The elastic modulus $E(\theta)$ and the temperature dependence parameter q_θ^e were determined from DMA data (Fig. 6 in Mulliken and Boyce, 2006) using E–θ curves at strain rates (10, 10^2 and $10^4 s^{-1}$) in the temperature range (293–380 K) . For each strain-rate value, an initial elastic modulus $E(\theta_0)$ and its corresponding q_θ^e value were determined by linear fitting $E(\theta)/E(\theta_0)$ against $(\theta-\theta_0)/\theta_0$ data and then averaging the resulting $(E(\theta_0), q_\theta^e)$ values. Lamé constants are obtained using the relationships $\mu^e = E/2(1+\nu)$ and $\lambda^e = \nu E/(1+\nu)(1-2\nu)$ assuming a constant Poisson's ratio $\nu = 0.38$. Seed values for the power-law exponents $\hat{\tau}$, m in the viscoplastic element where determined from the shear yield stress versus shear strain-rate curve (Fig.A.1 in Mulliken and Boyce, 2006) in the range 10^0–$10^4 s^{-1}$. Following, $\hat{\tau}$, m together with the strain softening f_f and $\hat{\epsilon}_p$ parameters were fine-tuned by fitting model simulations to the true stress–strain uniaxial compression curves at 10^2 and $10^3 s^{-1}$ in Mulliken (2004) using the MCalibration® commercial software by Veryst Engineering. The temperature dependence parameter for the viscoplastic element, q_θ^p was determined from the yield stress–temperature data in Bauwens-Crowet et al. (1972) by linear fitting $\sigma_Y(\theta)/\sigma_Y(\theta_0)$ against $(\theta-\theta_0)/\theta_0$ in the temperature range (293–380 K). The pressure dependence parameter $\tau_{t/c}$ was determined by taking the average of the tension/compression yield stress ratios from the yield stress–temperature data in Bauwens-Crowet et al. (1972) in the temperature range (293–380 K). The strain-hardening parameters μ and λ_L were determined by fitting model simulations to the true stress–strain uniaxial compression curve in Mulliken (2004) at 1 s^{-1} strain rate over the region dominated by strain hardening. The value for the inelastic heat fraction ω is taken directly from Bouvard et al. (2013). Dynamic coefficient of friction for the non-lubricated PC–Steel interface, μn_k is taken from Ludema and Bayer (1991). Tests using lubrication were modeled using frictionless contact. Thermal properties k and C_p were taken from the manufacturer technical data sheet.

References

Anand, L., Gurtin, M.E., 2003. A theory of amorphous solids undergoing large deformations, with application to polymeric glasses. International Journal of Solids and Structures 40 (6), 1465–1487.

Argon, A., 1973. A theory for the low-temperature plastic deformation of glassy polymers. Philosophical Magazine 28 (4), 839–865.

Argon, A.S., 2013. The Physics of Deformation and Fracture of Polymers. Cambridge University Press.

Arruda, E.M., Boyce, M.C., 1993. A three-dimensional constitutive model for the large stretch behavior of rubber elastic materials. Journal of the Mechanics and Physics of Solids 41 (2), 389–412.

Arruda, E.M., Boyce, M.C., Jayachandran, R., 1995. Effects of strain rate, temperature and thermomechanical coupling on the finite strain deformation of glassy polymers. Mechanics of Materials 19 (23), 193–212.

Bauwens-Crowet, C., Bauwens, J., Homes, G., 1972. The temperature dependence of yield of polycarbonate in uniaxial compression and tensile tests. Journal of Materials Science 7, 176–183.

Bergström, J., 2012. Polyumod—A Library of Advanced User Materials. Veryst Engineering, LLC, Needham, Mass, USA.

Bergström, J., Boyce, M., 1998. Constitutive modeling of the large strain time-dependent behavior of elastomers. Journal of the Mechanics and Physics of Solids 46 (5), 931–954.

Bergström, J., Rimnac, C., Kurtz, S., 2005. Molecular chain stretch is a multiaxial failure criterion for conventional and highly crosslinked UHMWPE. Journal of Orthopaedic Research 23 (2), 367–375.

Bergström, J.S., Bischoff, J.E., 2010. An advanced thermomechanical constitutive model for UHMWPE. International Journal of Structural Changes in Solids 2 (1), 31–39.

Bouvard, J., Francis, D., Tschopp, M., Marin, E., Bammann, D., Horstemeyer, M., 2013. An internal state variable material model for predicting the time, thermomechanical, and stress state dependence of amorphous glassy polymers under large deformation. International Journal of Plasticity 42 (0), 168–193.

Boyce, M.C., Parks, D., Argon, A., 1988. Large inelastic deformation of glassy polymers. part 1: Rate dependent constitutive model. Mechanics of Materials 7, 15–33.

Chang, F.-C., Wu, J.-S., Chu, L.-H., 1992. Fracture and impact properties of polycarbonates and mbs elastomer-modified polycarbonates. Journal of Applied Polymer Science 44 (3), 491–504.

Estevez, R., Tijssens, M., Van der Giessen, E., 2000. Modeling of the competition between shear yielding and crazing in glassy polymers. Journal of the Mechanics and Physics of Solids 48 (12), 2585–2617.

Faye, A., Parmeswaran, V., Basu, S., 2015. Mechanics of dynamic fracture in notched polycarbonate. Journal of the Mechanics and Physics of Solids 77, 43–60.

Fraser, R., Ward, I., 1977. The impact fracture behaviour of notched specimens of polycarbonate. Journal of Materials Science 12 (3), 459–468.

Gearing, B., Anand, L., 2004. Notch-sensitive fracture of polycarbonate. International Journal of Solids and Structures 41 (3), 827–845.

Gearing, B., Anand, L., 2004. On modeling the deformation and fracture response of glassy polymers due to shear-yielding and crazing. International Journal of Solids and Structures 41 (11), 3125–3150.

Gearing, B.P., 2002. Constitutive Equations and Failure Criteria for Amorphous Polymeric Solids Ph.D. thesis. Massachusetts Institute of Technology.

Hasan, O.A., Boyce, M.C., 1995. A constitutive model for the nonlinear viscoelastic viscoplastic behavior of glassy polymers. Polymer Engineering and Science 35 (4), 331–344.

Haward, R., Thackray, G., 1968. The use of a mathematical model to describe isothermal stress-strain curves in glassy thermoplastics. In: Proceedings of the Royal Society of London A: Mathematical, Physical and Engineering Sciences, Vol. 302. The Royal Society, pp. 453–472.

Hibbit, H., Karlsson, B., Sorensen, E., 2012. Abaqus User Manual. Simulia, Providence, RI.Version 6.12

Ishikawa, M., Narisawa, I., Ogawa, H., 1977. Criterion for craze nucleation in polycarbonate. Journal of Polymer Science 15, 1791–1804.

Kattekola, B., Ranjan, A., Basu, S., 2013. Three dimensional finite element investigations into the effects of thickness and notch radius on the fracture toughness of polycarbonate. International Journal of Fracture 181 (1), 1–12.

Lee, E.H., 1969. Elastic-plastic deformation at finite strains. Journal of Applied Mechanics 36 (1), 1–6.

Ludema, K.C., Bayer, R.G., 1991. Tribological Modeling for Mechanical Designers, STP 1105. ASTM International.

Meijer, H.E., Govaert, L.E., 2005. Mechanical performance of polymer systems: The relation between structure and properties. Progress in Polymer Science 30 (89), 915–938.Plenary Lectures World Polymer Congress, 40th IUPAC International Symposium on Macromolecules

Mulliken, A., Boyce, M.C., 2006. Mechanics of the rate-dependent elastic-plastic deformation of glassy polymers from low to high strain rates. International Journal of Solids and Structures 43, 1331–1356.

Mulliken, A.D., 2004. Low to High Strain Rate Deformation of Amorphous Polymers: Experiments and Modeling (Master's thesis). Masachussetts Institute of Technology.

Narisawa, I., Yee, A.F., 1993. Crazing and fracture of polymers. Materials Science and Technology 12, 699–765.

Newmann, L., Williams, J., 1980. A comparative study of the tensile and charpy impact tests from a fracture mechanics viewpoint. Polymer Engineering and Science 20 (8), 572–578.

Nimmer, R., Woods, J., 1992. An investigation of brittle failure in ductile notch-sensitive thermoplastics. Polymer Engineering and Science 32, 1126–1137.

Rietsch, F., Bouette, B., 1990. The compression yield behaviour of polycarbonate over a wide range of strain rates and temperatures. European Polymer Journal 26 (10), 1071–1075.

Smit, R., Brekelmans, W., Meijer, H., 2000. Predictive modelling of the properties and toughness of polymeric materials. Part I. Why is polystyrene brittle and polycarbonate tough? Journal of Materials Science 35 (11), 2855–2867.

Tiejun, W., Kishimoto, K., Notomi, M., 2002. Effect of triaxial stress constraint on the deformation and fracture of polymers. Acta Mechanica Sinica 18 (5), 480–493.

Wu, P.D., der Giessen, E.V., 1993. On improved network models for rubber elasticity an their applications to orientation hardening of glassy polymers. Journal of the Mechanics and Physics of Solids 41, 427–456.